RSC Advances

Time and energy conserving solution combustion synthesis of nano Li1.2Ni0.13Mn0.54Co0.13O2 cathode material and its performance in Li-ion batteries

Journal:	*RSC Advances*
Manuscript ID	RA-ART-09-2015-019096.R2
Article Type:	Paper
Date Submitted by the Author:	22-Oct-2015
Complete List of Authors:	Prakash, Annigere S.; Central Electrochemical Research Institute-Chennai Unit, Li-ion batteries K R, Prakasha; Central Electrochemical Research Institute-Chennai Unit, Li-ion batteries
Subject area & keyword:	Electrochemical energy < Energy

A table of contents entry: graphic

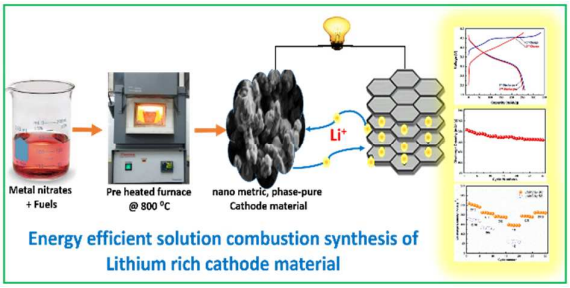

RSC Advances

ARTICLE

Time and energy conserving solution combustion synthesis of nano $Li_{1.2}Ni_{0.13}Mn_{0.54}Co_{0.13}O_2$ cathode material and its performance in Li-ion batteries

Received 00th January 20xx,
Accepted 00th January 20xx

DOI: 10.1039/x0xx00000x

www.rsc.org/

K. R. Prakasha,[ab] and A. S. Prakash[a]*

In search of an economic and energy conserving method for the synthesis of lithium rich cathode materials, an effective, quick and simple solution combustion method has been adopted for the synthesis of nano-sized $Li_{1.2}Ni_{0.13}Mn_{0.54}Co_{0.13}O_2$ phase, which is today's most praised positive electrode material for lithium ion batteries. This energy conservative route facilitates homogeneous atomic-level mixing of the precursors resulting in high quality product. In a short span of time, nano metric, phase-pure $Li_{1.2}Ni_{0.13}Mn_{0.54}Co_{0.13}O_2$ can be produced which is converted to electro active high performing cathode material on calcinations for less than 2 h at 850 °C. The synthesized lithium-rich phase delivers a reversible capacity of 260 mAh g^{-1} with superior cycling stability and exhibits good rate performance.

Introduction

In recent years there has been a great deal of interest in solid solutions of Li_2MnO_3 and $LiMO_2$ (M = Ni and Co) as high capacity cathode materials for Li-ion batteries.[1,2] These phases are generally designated as Li-rich phases and they exhibit high reversible capacity of 260 mAh g^{-1} with a good retention at high voltage as compared to other layered oxides.[3-5] In this class of Li-rich phases, the monoclinic Li_2MnO_3 structure closely resembles to the rhombohedral $LiMO_2$ structure. In Li_2MnO_3 structure, the Li^+ and Mn^{4+} ions occupy the transition metal layer and it can be reformulated as $Li[Li_{1/3}Mn_{2/3}]O_2$, whereas for the $LiMO_2$ structure, the transition metal layers are occupied by only transition metal ions. Thus, these two structures can be considered as layered α-$NaFeO_2$-type rock salt structures. The lithium ions in the transition metal layer result in cation ordering between transition metal and lithium layers forming the Li_2MnO_3 phase.[6]

The electrochemical performance crucially depends on physical (size, morphology) and chemical (Crystal structure, composition etc) nature of electrode materials which are directly influenced by synthetic techniques adopted.[7,8,9] For instance, Yao Fu *et al.* have described synthesis of Al doped $LiMn_2O_4$ truncated octahedron which provide exposure of highly active facets to enhance the capacity and rate capability; in addition Al in the structure hinder the Mn dissolution and hence demonstrate excellent capacity stability.[10] Similarly, several optimized synthetic methods have been reported for preparing high performing Li-ion battery electrode materials. In specific to Li-rich cathode materials, few papers are reported on improving the performance by adapting distinctive synthetic methods to yield kinetically suitable morphologies and sizes.[11] Wei *et al.* have reported high rate performance with a nano crystalline $Li_{1.2}Ni_{0.13}Mn_{0.54}Co_{0.13}O_2$ synthesised by hydrothermal

[a] CSIR–Network Institutes of Solar Energy (CSIR–NISE), CSIR Central Electrochemical Research Institute-Chennai unit, CSIR Madras Complex, Taramani, Chennai 600113, India

[b] Academy of Scientific and Innovative Research (AcSIR), CSIR-Madras Complex, , Taramani, Chennai 600113, India

method.[12] Wu *et al.* have followed co-precipitation method to synthesize spherical shaped $Li_{1.2}Ni_{0.13}Mn_{0.54}Co_{0.13}O_2$ with particle size of 5 µm.[13] He *et al.* were prepared high capacity (291 mAh g^{-1} at 20 mA g^{-1}) $Li_{1.2}Ni_{0.13}Mn_{0.54}Co_{0.13}O_2$ nano particles by polymer-pyrolysis method.[14] Radio frequency magnetron sputtering method has been reported by Yim *et al.* to fabricate $Li_{1.2}Ni_{0.13}Mn_{0.54}Co_{0.13}O_2$ thin film which is suitable positive electrode for all solid-state lithium-ion batteries.[15] Zheng *et al.* used sol–gel method to synthesize $Li_{1.2}Ni_{0.13}Mn_{0.54}Co_{0.13}O_2$ and investigated the effect of preparation methods on the structure, morphology and electrochemical performances.[11] Jafta *et al.* proposed one-step powder-forming Pechini method to synthesizes $Li_{1.2}Ni_{0.13}Mn_{0.54}Co_{0.13}O_2$ and its aluminium doped counterpart to compare their electrochemical performance.[16]

Among several synthesis techniques available for nano materials preparation in general, Solution combustion synthesis has gained considerable attention in recent years as it is simple, cost effective and quick process besides the prospect for scaling up.[17] The general difficulty often faced in solution combustion synthesis is the control ability over phases and morphologies of the products, as a result of inherent rapid and uncontrolled combustion reaction. Recently Wen *et al.* have reviewed the versatility of combustion synthesis for oxides with regular morphologies like tubes, wires, rods, nano belts and triangles by controlling the reaction dynamics.[18]

The present work is aimed at developing quick process to synthesize optimized nano-crystalline $Li_{1.2}Ni_{0.13}Mn_{0.54}Co_{0.13}O_2$ cathode material by urea-glycine-nitrate solution combustion method. Combustion process is a self-propagating exothermic redox reaction involving oxidizing metal nitrates and reducing organic fuel. The spontaneous exothermic heat liberated during the combustion reaction is utilized for the heat of formation of the complex oxides. As the solution combustion synthesis is a solution preparative technique and instantaneous, it yields well crystalline nano-particles with good homogeneity and high specific surface area which are desired parameters for high performing electrode materials.

Experimental Section

The $Li_{1.2}Ni_{0.13}Mn_{0.54}Co_{0.13}O_2$ cathode material was prepared using the urea-glycine-nitrate combustion method as follows. A stoichiometric quantity of $Ni(NO_3)_2{\cdot}6H_2O$, $Co(NO_3)_2{\cdot}6H_2O$, $Mn(NO_3)_2{\cdot}4H_2O$ and $LiNO_3$ [10% excess of $LiNO_3$ is added to compensate the Li loss during the combustion process] were dissolved in distilled water to which stoichiometric amount of glycine and urea (Glycine : urea in the ratio of 25:75 mole ratio) were added. The stoichiometry of oxidizing metal nitrates to reducing fuels (Glycine+Urea) is calculated as per the principle used in the propellant chemistry to balance the total oxidizing reducing valences.[19,20] The solution obtained was taken in alumina crucible and introduced to preheated muffle furnace at 800 °C. After ignition, the powder was ground and then re-heated at 850 °C for 2 h in air.

For comparison, $Li_{1.2}Ni_{0.13}Mn_{0.54}Co_{0.13}O_2$ phase is synthesized by conventional solid-state method as follows. The stoichiometric quantity of $Ni(C_2H_3O_2)_2{\cdot}4H_2O$, $Mn(C_2H_3O_2)_2{\cdot}4H_2O$, $Co(C_2H_3O_2)_2{\cdot}4H_2O$ and Li_2CO_3 (10% excess added to compensate the Li loss at high temperature) were mixed well by ball milling at 650 rpm for 1 h in an agate container using Fritsch Pulverisette-6 planetary mixer. The ball milled precursors was heated to 600 ^oC for 6 h, followed with calcination at 850 ^oC for 18 h with intermediate grinding.

The sample was phase characterized by X-ray diffraction (XRD) using a Bruker D8 Advance Da Vince diffractometer, with the Cu Kα radiation (λ_1 = 1.54056 Å, λ_2 = 1.54439 Å). The morphology and size of the powder was observed by scanning electron microscopy using (FESEM Carl Zeiss SUPRA55VP, Germany) and Transmission electron microscopy (TEM) studies were carried out with a Technai-20 G_2 microscope. The BET (Brunauer, Emmett and Teller) surface areas were estimated by N_2 adsorption method using Quantachrome ASiQwin instrument.

Electrochemical charge-discharge experiments were performed with swagelok-type cells assembled inside the argon-filled glove box. The working electrode was prepared by ball-milled mixture 80:20 (weight ratio) of active material and Super-P Li Carbon (Timcal Belgium) and Lithium disc as the counter/reference electrode. The typical active material loading was 5 to 6 mg/cm^2. The Whatman glass microfiber film was used as separator which was soaked in 1M $LiPF_6$ in solution of ethylene carbonate, dimethyl carbonate, and diethyl carbonate (2:1:2 ratio by volume) (LP 100) electrolyte. The galvanostatic charge-discharge cycling is performed at room temperature, at C/10 rate (C corresponding to the theoretical exchange of one mole of electron in 1 h) between 1.75

V to 4.8 V versus Li/Li^+. All the electrochemical experiments were carried out using VMP3Z biologic multi-channel potentiostat/galvanostat.

Results and Discussion

The properties of materials crucially depend on the synthetic conditions adopted. In a typical solution combustion synthesis, the exothermicity, duration of combustion reaction and volume of gaseous products are primarily controlled by the nature of fuel, oxidants and ratio of oxidant to fuel. Further the synthetic conditions like temperature of ignition, quantity of reactants used also influence the energetics of combustion reaction.

Thermodynamics of combustion synthesis

The combustion synthesis of $Li_{1.2}Ni_{0.13}Mn_{0.54}Co_{0.13}O_2$ using glycine alone as a fuel resulted in uncontrolled and violent reaction. On the other hand, urea does not yield sufficient exothermic heat to form the products. In this study, mixed fuel approach has been adapted to synthesize the Li-rich cathode material. Based on the thermodynamic calculations, the combustion process is optimized for the desired phase with right properties. The balanced chemical equation for the complete combustion reaction and their thermodynamic calculation for the individual reactions as well as for the mixed fuel are given below.

Reaction with Glycine as fuel:-

$$1.2LiNO_3+0.13Ni(NO_3)_2{\cdot}6H_2O+0.13Co(NO_3)_2{\cdot}6H_2O+0.54Mn(NO_3)_2{\cdot}4H_2O+1.55C_2H_5NO_2 \rightarrow Li_{1.2}Ni_{0.13}Mn_{0.54}Co_{0.13}O_2+2.2N_2\uparrow+7.6H_2O\uparrow+3.1CO_2\uparrow \quad (1)$$

Reaction with Urea as fuel:-

$$1.2LiNO_3+0.13Ni(NO_3)_2{\cdot}6H_2O+0.13Co(NO_3)_2{\cdot}6H_2O+0.54Mn(NO_3)_2{\cdot}4H_2O+2.33CO(NH_2)_2 \rightarrow Li_{1.2}Ni_{0.13}Mn_{0.54}Co_{0.13}O_2+3.7N_2\uparrow+8.4H_2O\uparrow+2.3CO_2\uparrow \quad (2)$$

Reaction with Mixed fuel (urea + glycine):-

The balanced chemical equations for the mixed fuel, Urea: Glycine in 75:25 ratio could be written as,

$$1.2LiNO_3+0.13Ni(NO_3)_2{\cdot}6H_2O+0.13Co(NO_3)_2{\cdot}6H_2O+0.54Mn(NO_3)_2{\cdot}4H_2O+1.75CO(NH_2)_2+0.388C_2H_5NO_2 \rightarrow Li_{1.2}Ni_{0.13}Mn_{0.54}Co_{0.13}O_2+3.3N_2\uparrow+8.2H_2O\uparrow+2.59CO_2\uparrow \quad (3)$$

By taking relevant thermodynamic data (Table S1 given in supporting information) of reactants and gaseous by-products from the literature,[21] the enthalpy of combustion reactions have been calculated assuming complete combustion as mentioned in above equations (1), (2) and (3).The enthalpy of combustion reaction has been determined using the relation:

$\Delta H_{combustion} = (\sum n\Delta H_f)_{products} - (\sum n\Delta H_f)_{reactants}$

For glycine:-

$\Delta H_{combustion}$ $= \Delta H_f(Li_{1.2}NMC) + \Delta H_f(\text{gas byproducts}) - \Delta H_f(\text{reactants})$

$= \Delta H_f(Li_{1.2}Ni_{0.13}Mn_{0.54}Co_{0.13}O_2) + (-3057.53) - (-1818.71)$

$= \Delta H_f(Li_{1.2}Ni_{0.13}Mn_{0.54}Co_{0.13}O_2) + (-1238.82)\ KJ\ mol^{-1}$

Total moles of gaseous by products:-12.9moles.

For urea:-

$\Delta H_{combustion} = \Delta H_f(Li_{1.2}Ni_{0.13}Mn_{0.54}Co_{0.13}O_2) + (-2943.14) - (-1775.67)$

$= \Delta H_f(Li_{1.2}Ni_{0.13}Mn_{0.54}Co_{0.13}O_2) + (-1167.47)\ KJ\ mol^{-1}$

Total moles of gaseous by products:-14.4moles.

For mixed fuels:-

$\Delta H_{combustion} = \Delta H_f(Li_{1.2}Mn_{0.54}Co_{0.13}Ni_{0.13}O_2) + (-2966.51) - (-1787.52)$

$= \Delta H_f(Li_{1.2}Mn_{0.54}Co_{0.13}Ni_{0.13}O_2) + (-1178.99)\ KJ\ mol^{-1}$

Total moles of gaseous by products:-14moles.

The exact values of enthalpy of combustion reaction in each cases mentioned above are not calculated due to the lack of thermodynamic statistics for $Li_{1.2}Ni_{0.13}Mn_{0.54}Co_{0.13}O_2$. However, since the ΔH_f of $Li_{1.2}Ni_{0.13}Mn_{0.54}Co_{0.13}O_2$ is constant for all the reactions, the energies of the three reactions can be understood by comparing the ΔH_f of the by-products. Although thermodynamic calculation based on heat of formation indicate slightly higher value for glycine and moderate for mixed fuels, it does not support the experimental observation that the reaction with glycine fuel alone is highly exothermic and violent. The exothermic heat of combustion reaction could also be influenced by the nature of complexation of organic fuel (ligand) with the cations.

Metal-ligand complexation

The fuel, glycine used here is an amino acid that forms complexes with 3d metal ions. In order to understand the nature of complexation process, the pH values of the reaction mixtures for glycine-metal nitrates, Urea-Metal nitrates and mixture of (urea+ glycine) – Metal nitrates have been measured. Details of the pH are given in Table S2 in supporting information. The pH of Glycine-Nitrates mixture is 3.05 that increases to 4.33 for Glycine+Urea. During preheating before the combustion, the solution pH could rise to as high as 6.74 which is, possibly attributed to part of urea undergoing instantaneous hydrolysis reaction. Generally, the zwitterions nature of the glycine depending on the pH of the solution is presents as protonated or deprotonated form. The

equilibrium between the protonates and deprotonates of glycine is shown in equation (4).

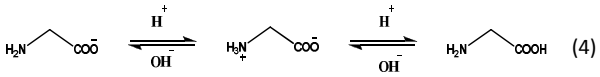

(4)

The complexation of glycine increased with decreasing the acidity of the solution hence, change in pH of nitrates-fuel solution alters the reaction kinetics of combustion reaction by playing a role in the formation of metal-ligand complex.

Product phase analysis

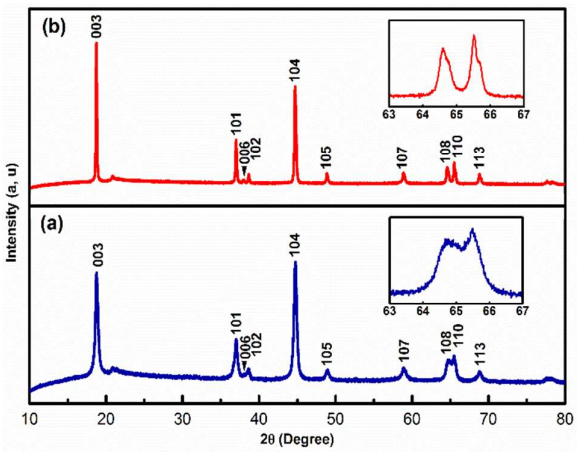

Fig. 1 X-ray diffraction patterns of solution combustion synthesized $Li_{1.2}Ni_{0.13}Mn_{0.54}Co_{0.13}O_2$ (a) as-prepared sample (b) reheated sample at 850 °C. The inset of figure shows

The XRD patterns of $Li_{1.2}Ni_{0.13}Mn_{0.54}Co_{0.13}O_2$ as-prepared and sample reheated at 850 °C for 2 h are shown in Fig. 1a and b. The patterns are indexed to a hexagonal α-$NaFeO_2$ structure with the $R\bar{3}m$ space group. The peaks observed between 20 and 30° (2θ) can be indexed considering a $\sqrt{3}a_{hex}$ x$\sqrt{3}b_{hex}$ superstructure in the *ab* transition metal planes as a result of ordering between the Li, Mn, Co, and Ni ions similar to the monoclinic Li_2MnO_3 structure (defined in the *C2/m* space group).[22,23] As can be seen from the Fig. 1a, the intensity of (003) peak is lower than the (104) peak and the integrated intensity ration of the (003) to (104) which can be used for quantification of cation mixing, is about 0.92 indicating undesirable cation mixing in the Li-layer. In addition, absence of clear splitting between (108)/(110) reflections shown as an inset in the figure also confirms high degree of cation mixing in the as prepared sample. Whereas in reheated pattern (shown in Fig. 1b) the clear splitting in peaks of (108)/(110) manifesting that the sample is well crystallized in the layered structure[24,25,26] and the integrated intensity ratio of the (003) to (104) is 1.40 which is more than 1.2, providing evidence that the cation mixing in the Li-layer is negligible for the reheated sample.[27,28]

Rietveld refined X-ray diffraction pattern of reheated $Li_{1.2}Ni_{0.13}Mn_{0.54}Co_{0.13}O_2$ sample using Fullprof software is shown in Fig. 2. The structure was refined using two-phase model consisting monoclinic Li_2MnO_3 (*C2/m* space group) and rhombohedral $LiNi_{0.33}Mn_{0.33}Co_{0.33}O_2$ ($R\bar{3}m$ space group) with assumption of ratio between the phases is 5:5. The refined structural parameters by the

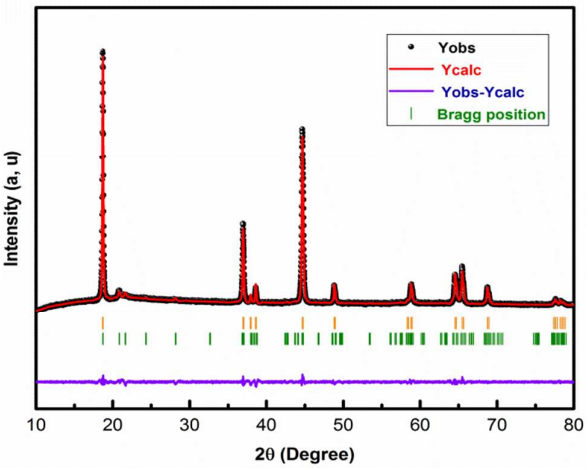

Fig. 2 Powder XRD pattern with Rietveld refinement of $Li_{1.2}Ni_{0.13}Mn_{0.54}Co_{0.13}O_2$ sample reheated at 850° C for 2 h. The experimental diffraction pattern (black dots), calculated patterns (red lines), the difference curve (green line) and Bragg diffraction positions (blue ticks for $R\bar{3}m$ space group and red ticks for *C 2/m* space group) are presented.

Rietveld analysis are listed in Table S3 given in the supporting information. The X-ray diffraction pattern of solid state prepared sample is similarly refined using the two-phase model as described before. Rietveld refined X-ray diffraction pattern of solid state synthesized $Li_{1.2}Ni_{0.13}Mn_{0.54}Co_{0.13}O_2$ sample is displayed in Fig S1 (ESI). The refined lattice parameters for solid state synthesised sample are also given in Table S3

Microscopic analysis

Fig. 3a displays the morphology of reheated $Li_{1.2}Ni_{0.13}Mn_{0.54}Co_{0.13}O_2$ sample investigated by FESEM. The image indicates well defined morphology of the sample with dimensions ranging between 100-300 nm. The homogeneous distribution of the transition elements in the sample has been clearly revealed through

elemental mapping displayed in Fig. 3b-d. The EDS profile seen from Fig. 3e shows the transition metal composition having the atomic ratio between Ni:Mn:Co as 16.53%, 66.8% and 17.39% which is quite near in concord with the targeted composition of the phase i.e. 0.13:0.54:0.13 ratios respectively. It is clear from these studies, the sample prepared by solution combustion method is composed of well-defined morphology with particle sizes of around 100–300 nm. On the other hand the FESEM image of solid state prepared sample (shown as the inset in the Fig S1) displays the morphology with particle size were measured to be 1 to 3 µm. The active surface area of combustion derived nano phase measured by Brunauer, Emmet and Teller (BET) method is 5.431m^2 g^{-1}. The active surface area of solid state derived sample is 0.6 m^2 g^{-1}.

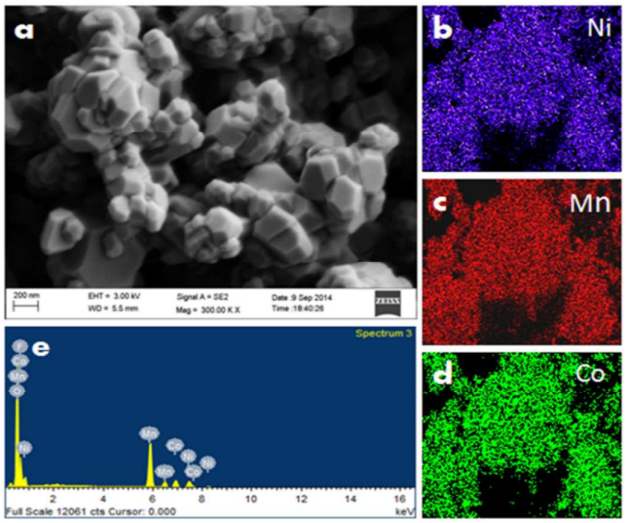

Fig. 3 FESEM and EDS Characterization of $Li_{1.2}Ni_{0.13}Mn_{0.54}Co_{0.13}O_2$ reheated sample: (a) FESEM image and mapping revealing the presence of (b) nickel, (c) manganese, (d) cobalt, along with (e) EDS profile.

The high resolution TEM images and SAED pattern of both as prepared and reheated $Li_{1.2}Ni_{0.13}Mn_{0.54}Co_{0.13}O_2$ samples are presented in Fig. 4a-f. The micrograph shows the particles are agglomerated with the size in the range of 50-100 nm for as-prepared sample (Fig. 4a), whereas the particle size of reheated sample increases to about 100-300 nm (Fig. 4b) due to sintering process. The Fig. 4c and d shows the high resolution image of as-prepared prepared and heated sample respectively. The interference fringe spacing calculated for both the samples are around 4.7 A° which is in concurrence with d-spacing of (003) plane with a rhombohedral structure. The SAED pattern recorded on the agglomerate of as-prepared sample show a diffraction ring pattern (Fig. 4e) typical of polycrystalline sample while, SAED of individual crystallite of heated sample exhibits single crystal like spot pattern. Both the patterns are indexed in $R\bar{3}m$ space group.

Electrochemical performances

Cyclic voltammogram of $Li_{1.2}Ni_{0.13}Mn_{0.54}Co_{0.13}O_2$ is presented in Fig. 5. During the first charge, two oxidation peaks are observed. The broad peak around 4.0 V corresponds to the oxidation of the transition metals (Ni^{2+} →Ni^{4+} and Co^{3+} →Co^{4+}),[29] which is followed with a sharp peak around 4.6 V that is attributed to the loss of oxygen with Li extraction.[30] During the following discharge, the peaks around 4.3 V and 3.7 V corresponds to the reduction of Ni^{4+}

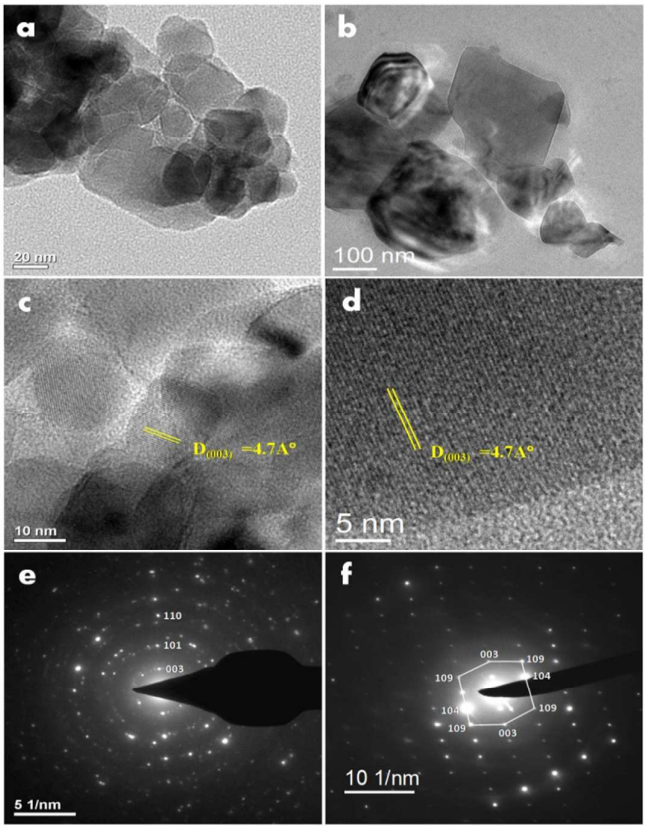

Fig. 4 TEM images of $Li_{1.2}Ni_{0.13}Mn_{0.54}Co_{0.13}O_2$ as-prepared and reheated sample (a, b), High resolution TEM images (c, d) and Selected area electron diffraction patterns (e, f).

and Co^{4+}, while the peak around at 3.3 V is attributed to the reduction of Mn ions (Mn^{4+} →$Mn^{(4-x)+}$ (0 < x < 1)).[31] In the subsequent cycles, three peaks are observed during charge (marked as 1, 2 and 3) which corresponds to the three reduction peaks (marked as 1*, 2* and 3*) in the discharge cycles indicate the

complete reversible process. Oxidation peaks at 3.8 V (2) and 4.4 V (1) corresponds to the Ni^{2+} and Co^{3+} oxidation[32] and the peak below 3.5 V (3,3*) assigned to the reversible oxidation of the Mn^{3+}/Mn^{4+}.[14] Fig. 6 shows the first and second charge discharge profiles of the $Li_{1.2}Ni_{0.13}Mn_{0.54}Co_{0.13}O_2$ cathode material at a rate of C/10 in the voltage window of 1.75 to 4.8 V. During the first charge cycle a sloping region below 4.4 V corresponds to the oxidation of the transition metals ($Ni^{2+} \rightarrow Ni^{4+}$ and $Co^{3+} \rightarrow Co^{4+}$) as discussed in CV.

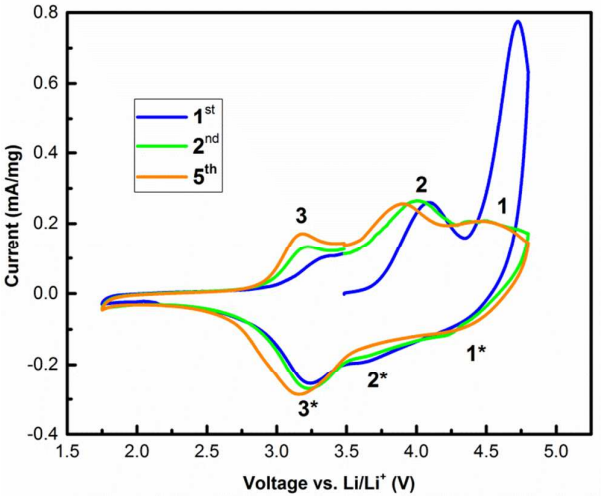

Fig. 5 Cyclic voltammogram of $Li_{1.2}Ni_{0.13}Mn_{0.54}Co_{0.13}O_2$ cycled between 1.75 and 4.8 V at a scan rate of 0.1 mV s^{-1}.

The long plateau that began around 4.4 to 4.6 V corresponds to removal of lithium from the transition metal layer phase which is also accompanied by the removal of oxygen from the structure.[33,34] During the second charge the absence of voltage plateau above 4.4 V is attributed to structural transformation associated with the oxygen loss as described before. The initial charge and discharge capacities are 334 and 260 mAh g^{-1}, respectively. The large irreversible capacity of about 70 mAh g^{-1} observed in the first cycle is in agreement with previous reports for Li-rich phase[35] and it is attributed to structural transformations and oxygen loss in the Li-rich phase.[30] The well-exposed nano particles can facilitate easy oxygen loss from the layered lattice[36,37] and provide shorter diffusion pathway for Li-ions. The capacity of first discharge and consecutive cycles is attributed to the redox of 3d metals as discussed in CV. Fig. 7 shows the profile of the cycle number vs discharge capacity of the material. It delivers the first discharge capacity around 260 mAh g^{-1}, then gradual decreasing of the discharge capacity. The reversible capacity is around 204 mAh g^{-1} after 30 cycles, which is about 82.9 % of the capacity at C/10-rate.

Diffusion time of lithium ions in electrode particle is proportional to the square of diffusion path length. Therefore the reduction of particle sizes is expected to enhance the intercalation kinetics and hence exhibit high rate performance. To evaluate the rate performance of nano metric $Li_{1.2}Ni_{0.13}Mn_{0.54}Co_{0.13}O_2$, galvanostatic cycling at different current densities were conducted and the data are compared with the micron sized powder which is obtained with the conventional solid state synthesis. Fig. 8 shows

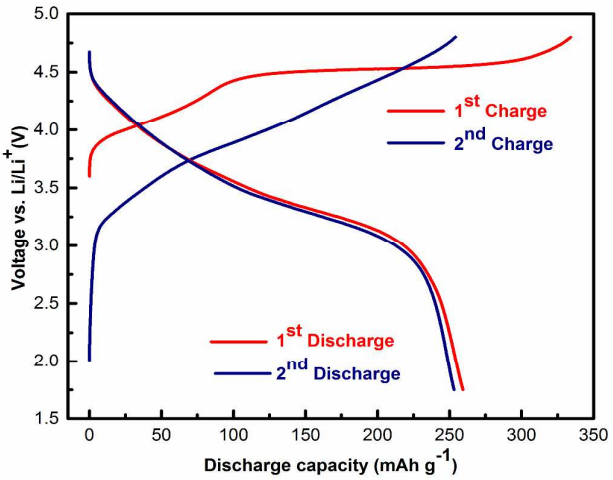

Fig. 6 First and second charge–discharge profile of $Li_{1.2}Ni_{0.13}Mn_{0.54}Co_{0.13}O_2$ cycled in the voltage range of 1.75–4.8 V at a rate of C/10.

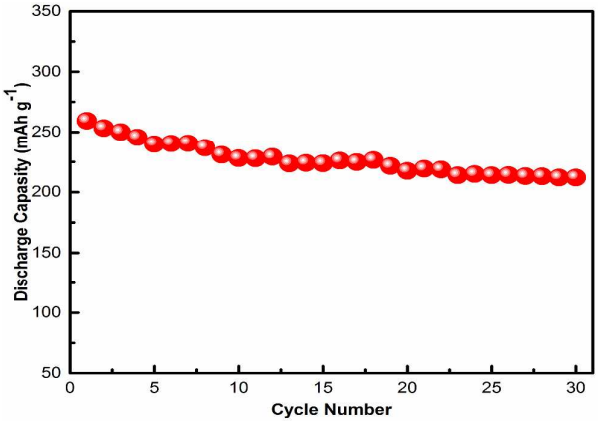

Fig. 7 The profile of the cycle number vs discharge capacity performances of the $Li_{1.2}Ni_{0.13}Mn_{0.54}Co_{0.13}O_2$ cycled between 1.75 and 4.8 V at C/10 rate.

rate capability plot for nano and micron sized $Li_{1.2}Ni_{0.13}Mn_{0.54}Co_{0.13}O_2$ phase vs Li half-cell cycled under identical conditions. The solution combustion synthesized nano material delivers the excellent discharge capacities of 260, 204, 191 and 148 mAh g^{-1} at C/10, C/5, C/2 and 1C rates respectively. Whereas Solid-state synthesized phase delivers 176, 132 and 60 mAh g^{-1} at C/10,

C/5, and 1C rate respectively. This large difference in the rate performance between solid state synthesized sample and solution combustion synthesized sample is mainly attributed to the well crystalline nano phase with minimum cation mixing, which determine the better lithium-ion diffusion in the material. The work presented in this manuscript is an offshoot of scaling up process being developed for large scale synthesis of Li-ion battery electrode materials by continuous spray combustion process.

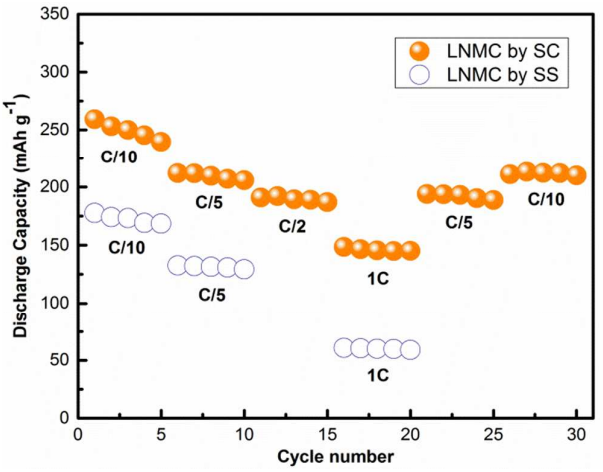

Fig. 8 Comparison of rate capability values for $Li_{1.2}Ni_{0.13}Mn_{0.54}Co_{0.13}O_2$ synthesized by solution combustion method and solid state method at different rates in the voltage range of 1.75 to 4.8 V.

Detailed studies on scaling up process will be reported in future publication.

Conclusions

The solution combustion method has been introduced as an energy-conservation route for the synthesis of nano structured $Li_{1.2}Ni_{0.13}Mn_{0.54}Co_{0.13}O_2$ positive electrode material for the first time. The required degree of cation ordering (less than 5%) in the synthesised nano phase can be achieved by heating to high temperature for a short span of time without compromising the particle growth. The nano sized lithium rich phase has demonstrated a reversible capacity of 260 mAh g^{-1} as a positive electrode material in Li-ion battery and exhibits good cycle life too. As a proof of concept, although, the process is demonstrated here for the Li-rich phase, it can as well be extended to synthesize many other layered materials for battery application. Further, solution combustion synthesis is an attractive method as it is cost effective and quick process besides having the prospect for scaling up.

Acknowledgements

The authors thank the Council of Scientific and Industrial Research (CSIR), India for support of this work under TAPSUN project of CSIR. Mr K. R. Prakasha thanks CSIR for CSIR-UGC Fellowship. The authors thank the Central Instrumentation Facility, CECRI, Karaikudi, and the CSIR Innovation complex facilities, CSIR Madras Complex, Chennai, for providing characterization facilities.

Notes and references

1. Z. Lu, D. D. Mac Niel and J.R. Dahn, Electrochem. Solid-State Lett., 2001, **4**, A191
2. Y. J. Park, Y. S. Hong, X. Wu, K. S. Ryu and S. H. Chang, *J. Power Sources,* 2004, **129**, 288.
3. C. S. Johnson, N. Li, C. Lefief, J. T. Vaughey and M. M. Thackeray, *Chem. Mater.,* 2008, **20**, 6095.
4. M. M. Thackeray, C. S. Johnson, J. T. Vaughey, N. Li and S. A. Hackney, *J. Mater. Chem.,* 2006, **15**, 2257.
5. T. Ohzuku, M. Nagayama, K. Tsuji and K. Ariyoshi, *J. Mater. Chem.,* 2011, **21**, 10179.
6. C. R. Fell, M. Chi, Y. S. Meng and J. L. Jones, *Solid State Ionics.,* 2012, **207**, 44.
7. M. G. Kim, M. Jo, Y. S. Hong and J. Cho, *Chem. Commun.,* 2009, 218.
8. H. Jiang , Y. Fu , Y. Hu , C. Yan , L. Zhang , P. S. Lee and C. Li, *Small*, 2014, **10**, 1096
9. Y. Fu, H. Jiang, Y. Hu, L. Zhang and C. Li *J. Power Sources,* 2014, **261**, 306.
10. Y. Fu, H. Jiang, Y. Hu, Y. Dai, L. Zhang, and C. Li*, Ind. Eng. Chem. Res,* 2015, **54**, 3800.
11. J. M. Zheng, X. B. Wu and Y. Yang, *Electrochim. Acta.,* 2011, **56**, 3071.
12. X. Wei, S. Zhang, Z. Du, P. Yang, J. Wang and Y. Ren, *Electrochim. Acta.,* 2013, **107**, 549.
13. Y. Wu and A. Manthiram, *Electrochem. Solid-State Lett.,* 2006, **9**, A221.
14. W. He, J. Qian, Y. Cao, X. Ai and H. Yang, *RSC Adv.,* 2012, **2**, 3423.

15. H. Yim, W. Y. Kong, Y. C. Kim, S. J. Yoonand J. W. Choi, *J. Solid State Chem.,* 2012, **196**, 288.
16. C. J. Jafta, K.I. Ozoemena, M.K. Mathe and W.D. Roos, *Electrochim. Acta.,* 2012, **85**, 411.
17. S. T. Aruna, A. S. Mukasyan, *Curr. Opin. Solid State and Mater. Sci.,* 2008, **12**, 44.
18. W. Wen and Jin-Ming Wu, *RSC Adv.,* 2014, **4**, 58090.
19. A. S. Prakash, A. M. A.Khadar, K. C. Patil and M. S. Hegde, *J. Mater. Synth. Process.,* 2002, **10**, 135.
20. C. Shivakumara, M. B. Bellakki, A. S. Prakash and N. Y. Vasanthacharya, *J. Am. Ceram. Soc.,* 2007, **90**, 3852.
21. J. A. Dean, *Lange's Handbook of Chemistry* (*13th ed.*). McGraw-Hill, New York, 1985.
22. F. Weill, N. Tran, L. Croguennec and C. Delmas, *J. Power Sources,* 2007, **172**, 893
23. A. Boulineau, L. Croguennec, C. Delmas and F. Weill, *Chem. Mater.,* 2009, **21**, 4216
24. A. Rougier, P. Gravereau and C. Delmas, *J. Electrochem. Soc.,* 1996, **143**, 1168.
25. K. S. Park, M. H. Cho, S. J. Jin and K. S. Nahm, *Electrochem. Solid-State Lett.,* 2004, **7**, A239.
26. Z. H. Lu, L.Y. Beaulieu, R. A. Donaberger, C. L. Thomas and J. R. Dahn, *J. Electrochem. Soc.,* 2002, **149**, A778.
27. B. J. Hwang, R. Santhanam and C. H. Chen, *J. Power Sources,* 2003, **114**, 244.
28. T.A. Arinkumar, Y. Wu and A. Manthiram, *Chem. Mater.,* 2007, **19**, 3067.
29. W. Liu, G. Fang, B. Xia, H. Sun, S. Kaneko, and D. Li, *RSC Adv.,* 2013, **3**, 15630.
30. B. H. Song, M. O. Lai and L. Lu, *Electrochim. Acta.,* 2012, **80**, 187.
31. B. H. Song, Z. W. Liu, M. O. Lai and L. Lu, *Chem. Phys.,* 2012, **14**, 12875.
32. Z. H. Lu and J. R. Dahn, *J. Electrochem. Soc.,* 2002,**149**, A815.
33. H. Yu, Y. Wang, D. Asakura, E. Hosono, T. Zhang and H. Zhou, *RSC Adv.,* 2012, **2**, 8797.
34. J. M. Kim, N. Kumagai and H. T. Chung, *Electrochem. Solid-State Lett.,* 2006, **9**, A494.
35. M. M. Thackeray, S. H. Kang, C.S. Johnson, J. T. Vaughey and S. A. Hackney, *Electrochem. Commun.,* 2006, **8**, 1531.
36. Z. Q. Deng and A. Manthiram, *J. Phys. Chem. C,* 2011, **115**, 7097.
37. P. Xiao, Z. Q. Deng, A. Manthiram and G. Henkelman, *J. Phys. Chem. C,* 2012, **116**, 23201.